ELEMENTA
Science of the Anthropocene

Ström, J, et al. 2022. Snow albedo and its sensitivity to changes in deposited light-absorbing particles estimated from ambient temperature and snow depth observations at a high-altitude site in the Himalaya. *Elem Sci Anth*, 10: 1. DOI: https://doi.org/10.1525/elementa.2021.00118

RESEARCH ARTICLE

Snow albedo and its sensitivity to changes in deposited light-absorbing particles estimated from ambient temperature and snow depth observations at a high-altitude site in the Himalaya

Johan Ström[1], Jonas Svensson[2,3,*], Henri Honkanen[4], Eija Asmi[2], Nathaniel B. Dkhar[5], Shresth Tayal[6,7], Ved P. Sharma[6,7], Rakesh Hooda[2], Outi Meinander[2], Matti Leppäranta[4], Hans-Werner Jacobi[3], Heikki Lihavainen[2,8], and Antti Hyvärinen[2]

Snow darkening by deposited light-absorbing particles (LAP) accelerates snowmelt and shifts the snow melt-out date (MOD). Here, we present a simple approach to estimate the snow albedo variability due to LAP deposition and test this method with data for 2 seasons (February–May 2016 and December 2016–June 2017) at a high-altitude valley site in the Central Himalayas, India. We derive a parameterization for the snow albedo that only depends on the daily observations of average ambient temperature and change in snow depth, as well as an assumed average concentration of LAP in snow precipitation. Linear regression between observed and parameterized albedo for the base case assuming an equivalent elemental carbon concentration $[EC_{eq}]$ of 100 ng g^{-1} in snow precipitation yields a slope of 0.75 and a Pearson correlation coefficient r^2 of 0.76. However, comparing the integrated amount of shortwave radiation absorbed during the winter season using observed albedo versus base case albedo resulted in rather small differences of 11% and 4% at the end of Seasons 1 and 2, respectively. The enhanced energy absorbed due to LAP at the end of the 2 seasons for the base case scenario (assuming an $[EC_{eq}]$ of 100 ng g^{-1} in snow precipitation) was 40% and 36% compared to pristine snow. A numerical evaluation with different assumed $[EC_{eq}]$ in snow precipitation suggests that the relative sensitivity of snow albedo to changes in $[EC_{eq}]$ remains rather constant for the 2 seasons. Doubling $[EC_{eq}]$ augments the absorption by less than 20%, highlighting that the impact on a MOD is small even for a doubling of average LAP in snow precipitation.

Keywords: Snow albedo, Light-absorbing particles, Himalaya

1. Introduction

The seasonal snow in the Himalayas is an integral component of the regional hydrological cycle, with the timing of the melting phase being crucial for the supply of water resources and with growing importance at increasing altitudes (e.g., Armstrong et al., 2019; Mimeau et al., 2019). Moreover, replacing a bright snow surface with a darker soil surface drastically changes the radiative balance, affecting the local climate. The albedo of snow has a key role in the energy balance of the snowpack and is one of the main regulators of snowmelt (Cuffey and Paterson, 2010). Strongly dependent on the microphysical properties of snow (e.g., snow liquid water content, grain size, and shape; Aoki et al., 2003), the albedo is also affected by the presence of light-absorbing particles (LAP; Warren and Wiscombe, 1980). Light-absorbing carbonaceous particles are part of LAP that can be transported from distant source regions before being deposited to snow. Originating mostly from anthropogenic emissions, black carbon and brown carbon (BC, BrC) are associated with the combustion of biomass and fossil fuels, although natural wildfires can also be a significant source of BC and BrC in Asia. Another important LAP in Himalayan snow is mineral dust (MD), with nearby natural emissions sources. Determining the partitioning of these LAP constituents in

[1] Department of Environmental Science, Stockholm University, Stockholm, Sweden
[2] Atmospheric Composition Research, Finnish Meteorological Institute, Helsinki, Finland
[3] Institute for Geosciences and Environmental Research, University Grenoble Alpes, CNRS, IRD, INP-G, Grenoble, France
[4] Institute for Atmospheric and Earth System Research, Faculty of Science, University of Helsinki, Helsinki, Finland
[5] Mu Gamma Consultants Pvt. Ltd., Gurugram, Haryana, India
[6] The Energy and Resource Institute, New Delhi, India
[7] The Energy and Resource Institute School of Advanced Studies, New Delhi, India
[8] Svalbard Integrated Arctic Earth Observing System, Longyearbyen, Norway

* Corresponding author:
Email: jonas.svensson@fmi.fi

Downloaded from http://online.ucpress.edu/elementa/article-pdf/10/1/00118/716484/elementa.2021.00118.pdf by guest on 14 August 2024

Himalayan snow is of particular interest with regard to a potential human influence on the regional climate and hydrological cycle.

Snow darkening by BC in the Himalayas has been reported to vary regionally, seasonally, and with altitude in observations (e.g., Gertler et al., 2016; Li et al., 2018). This has also been reported in simulations, which further reported that the snow albedo reductions and surface radiative effects mainly accompany the BC content (He et al., 2018). Additionally, the authors present BC-induced radiative effects in the range of 0.7–58.4 W m^{-2} for the Tibetan Plateau. The other main LAP constituent, MD, was recently identified as the dominating light absorber in the snow above 4,000 m altitude for high-mountain Asia (Sarangi et al., 2020). In contrast, Schmale et al. (2017) and Li et al. (2018) reported BC as the main particle absorber in measurements of glacier snow samples from Kyrgyzstan, Central Asia, and the Zhadang glacier in the Tibetan Plateau, respectively. In terms of snow cover duration, BC and MD have been found to decrease it by 1 to 10 days for different snow water equivalents (SWE) and shortwave radiation scenarios (Jacobi et al., 2015; Zhang et al., 2018).

In recent years, different sophisticated modeling tools have been developed in order to account for many of the complex interactions between LAPs and snow (e.g., Jacobi et al., 2015; Tuzet et al., 2017; Skiles and Painter, 2019; Tuzet et al., 2020; Niwano et al., 2021). These models are very complex and commonly require extensive data sets to force the models (including detailed meteorological data) and to validate the results (including frequent temporal snow pit observations). Complex environments with high spatial variability, limited access, and convoluted series of events, such as precipitation and melt, strongly limit the access to comprehensive data sets in high-altitude regions that can be used to drive such models. Typically, the models are validated by reproducing the observed conditions such as albedo and snow depth (SD). This is followed by removing or adding perturbations to LAP in snow and the net results are compared.

Here, we study if simplifying the complex description of the evolution of surface snow albedo by making some key assumptions and parameterize processes using proxy variables delivers useful results. We focus on the observed ambient temperature, variation in daily SD (effectively the derivative), and an assumed constant LAP concentration in snow precipitation as key parameters. Especially in remote areas, under harsh conditions with limited possibilities for measurements, our simplified approach to emulate surface snow albedo may be an option to estimate local radiative forcing due to LAP. Moreover, we used this simplified approach to explore the relation between LAP in precipitating snow and seasonally integrated absorbed short wave radiation. The observations used in this study include 2 seasons of automatic weather station (AWS) data from the Sunderdhunga valley at about 4,700 m altitude in Central Himalaya. Fundamental for the approach is also the previously characterized LAP deposition in glacier snow from the same valley (Svensson et al., 2021). To calculate the albedo reduction originating from the LAP in snow, we utilize the parametric relation by Pedersen et al. (2015). Their formulation is spectrally dependent on 2 parameters: (1) the ECeq concentration (referring to an operationally defined elemental carbon [EC] as proxy for BC, and where eq represents the equivalent absorption including BC and other light-absorbing non-BC constituents) in the surface snow and (2) the equivalent radii, r_e, of the snow grains. With neither of these parameters directly measured at our site in the Sunderdhunga valley, they are here derived from other available observations and assumptions.

This study is presented in 2 main sections. The methodology and derivation of the parametric model are described in Section 2 (summarized in a flow chart in Figure S1), while the results and comparison with observations are presented in Section 3. The methodology section is further subdivided by presenting the key observations, procedure for calculating LAP concentration in the surface snow, snow grain size, surface snow albedo, as well as the influence from ground albedo on the snow albedo. The result section presents both the observed and parameterized surface snow albedo. These are used to calculate the seasonally integrated absorbed short wave energy and the results are compared and discussed. Finally, the sensitivity to the seasonally absorbed short wave radiation through changes in LAP is explored.

2. Methods

2.1. Observations

2.1.1. Automatic weather station

The AWS observations are from the immediate vicinity (approximately 100 m) of the glacier ablation zone of Durga Kot glacier in the Sunderdhunga valley, northern India (30° 12′58.3″ N, 79° 51′32.4″ E, 4,700 masl), further described by Svensson et al. (2018; 2021). Two seasonal snow cover periods are utilized here (indicated by arrows in **Figure 1**), lasting between February 6, 2016, and May 22, 2016 (Season 1), and between December 24, 2016, and June 1, 2017 (Season 2). The AWS is equipped with instrumentation for air temperature (T_a), relative humidity (HC2S3-L Temperature and relative humidity probe manufactured by Rotronic, with 41303-5A radiation shield), upward and downward broadband short waves (SW_u, SW_d) and longwave radiation (LW_u, LW_d) (CNR4 Four-component net radiometer manufactured by Kipp & Zonen), SD (Campbell Scientific SR50A-L Ultrasonic Distance Sensor), wind speed (U), and wind direction (05103-L Wind monitor manufactured by R. M. Young). Data were logged every 10 min and screened for inconsistencies, which may arise, for example, from snow covering the sensors. Subsequently, the data were averaged over each day. To reduce the influence from noise and better capture representative values, the daily median values were used for albedo and SD instead of averages. The time series of albedo and SD covering the entire measuring period from September 22, 2015, to October 31, 2017, are presented in **Figure 1**. The AWS data are presented as time series in Figure S2.

Precipitation was not directly measured but was estimated using the method described in Svensson et al.

Downloaded from http://online.ucpress.edu/elementa/article-pdf/10/1/00118/716484/elementa.2021.00118.pdf by guest on 14 August 2024

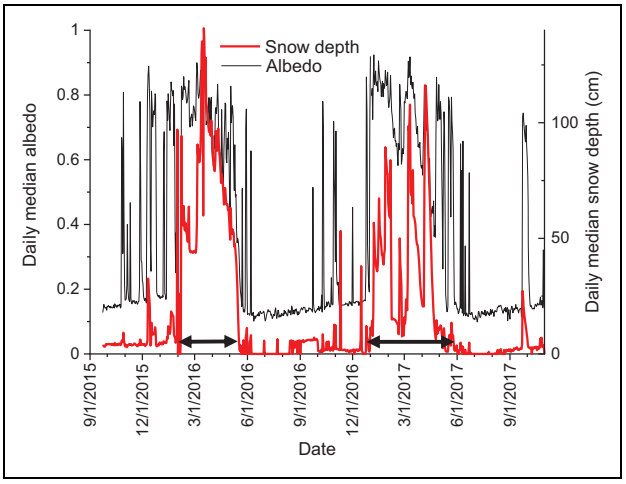

Figure 1. Measured daily median albedo and snow depth from September 22, 2015, to October 31, 2017. The 2 periods with a seasonal snow cover analyzed in this article are indicated with the black double arrow lines. DOI: https://doi.org/10.1525/elementa.2021.000118.f1

(2021) yielding an estimate of the amount of precipitation in mm SWE. The positive changes in SD (SD^+) were integrated over Seasons 1 and 2, and the density of the new snow was assumed to be 100 kg m^{-3} (Helfricht et al., 2018). The estimated total precipitation for Season 1 and Season 2 were 290 and 460 mm, respectively. As the snow cover appears and disappears over a season, the integrated decreases in SD, $\sum(SD^-)$, will be equal to $\sum(SD^+)$, but with opposite sign.

2.1.2. Deposition of LAP

A central component of the approach presented here are the original LAP observations reported in Svensson et al. (2021). The authors showed that LAP in young snow (interpreted as snow from the current winter season; here denoted as snow precipitation), sampled at Durga Kot and the neighboring Bhanolti glacier at a distance about 1–2 km southwest from the AWS at about 5,000 m altitude, can be described by a characteristic constant wet deposition of EC. The numeric value was about 50 μg m^{-2} mm^{-1}. This is the same as if each gram of precipitating water contains 50 ng of EC (or ppb) resulting in a total wet deposition of 14,500 μg m^{-2} and 23,000 μg m^{-2} at the end of Seasons 1 and 2, respectively.

For both winter seasons, the dry deposition of EC likely contributed small amounts to the overall deposition of EC as proposed in Svensson et al. (2021). Using a dry deposition velocity of BC of 0.3 mm s^{-1} (Emerson et al., 2018) and an atmospheric concentration of 0.3 μg m^{-3}, reported at the Nepal Pyramid station during the premonsoon (Bonasoni et al., 2010), the estimated dry deposition corresponds to approximately 850 and approximately 1250 μg m^{-2} EC for Seasons 1 and 2, respectively. A comparison with the EC wet deposition suggests that EC dry deposition is on the order of only 5%–6% of the total EC deposition. Therefore, we conclude that wet deposition dominates removal of EC from the atmosphere and the deposition at the location during the analyzed periods, which represent the main precipitation periods of the year for this site.

Svensson et al. (2021) also concluded that light absorption by MD was typically equal to EC. Light absorption by organic carbon (OC) was not determined in their study. Although in some areas with strong algae growth, OC may reduce the albedo significantly (e.g., Onuma et al., 2020). Based on the results reported by Svensson et al. (2021), we formulate a base case scenario, where the deposition of equivalent EC (EC_{eq}) is taken as 2 times the value for EC to include the contribution from MD. Hence, the numerical LAP value for our base case is 100 ng g^{-1} in precipitating snow considering only BC and MD.

2.2. Deriving estimated values for LAP concentration and snow grain effective radii

The dependent variable in the formulation by Pedersen et al. (2015) is the product between $LAP^{0.5}$ (LAP expressed as the equivalent EC concentrations at the snow surface) and the snow grain size, r_e (cf. Equation 9). As these 2 variables are not specifically observed during our study, they must be derived instead. In Section 2.2.1, we introduce the first simplification in our approach to arrive at a LAP surface concentration, and in the following Section 2.2.2, we introduce the second important simplification with respect to r_e.

2.2.1. Estimating LAP surface concentration

The first important variable of two in the formulation by Pedersen et al. (2015) is the LAP concentration in the surface snow layer. This introduces the first simplification in our approach, where it is assumed that as snow melts, LAP from the melted snow accumulates over a characteristic depth (d) in the surface layer. Although there are reports that suggests that LAP percolates through the snow during the intense melting phase (e.g., Sterle et al., 2013; Lazarcik et al., 2016), the majority of the literature describe a surface accumulation throughout the snow season (e.g., Flanner et al., 2007; Xu et al., 2012; Doherty et al., 2013; Svensson et al., 2016). We will return to the numeric value of d in Section 2.5 below. Our second assumption is that as snow accumulates, LAP concentration is given by the average concentration in snow precipitation. For our base case, this is 100 μg EC_{eq} m^{-2} per mm^{-1} or 100 ng g^{-1}, based on Svensson et al. (2021) cf. Section 2.1.2. Since direct measurements of precipitation or snowmelt are not available at our study site, we have used the observed change in SD as proxy for this (described above in Section 2.1.1). The surface concentration of LAP over depth layer d for a seasonal snow cover is therefore given by the 2 assumptions stated above; that LAP from melted snow accumulates in a surface layer and that LAP concentration in snow precipitation is constant. Thus, in the first case, for an increasing SD (SD^+), the surface concentration is simply equal to an average snow precipitation concentration of LAP according to,

$$[EC_{eq}]_{surf\ n} = [EC_{eq}]_{sp}, \quad (1)$$

Downloaded from http://online.ucpress.edu/elementa/article-pdf/10/1/00118/716484/elementa.2021.00118.pdf by guest on 14 August 2024

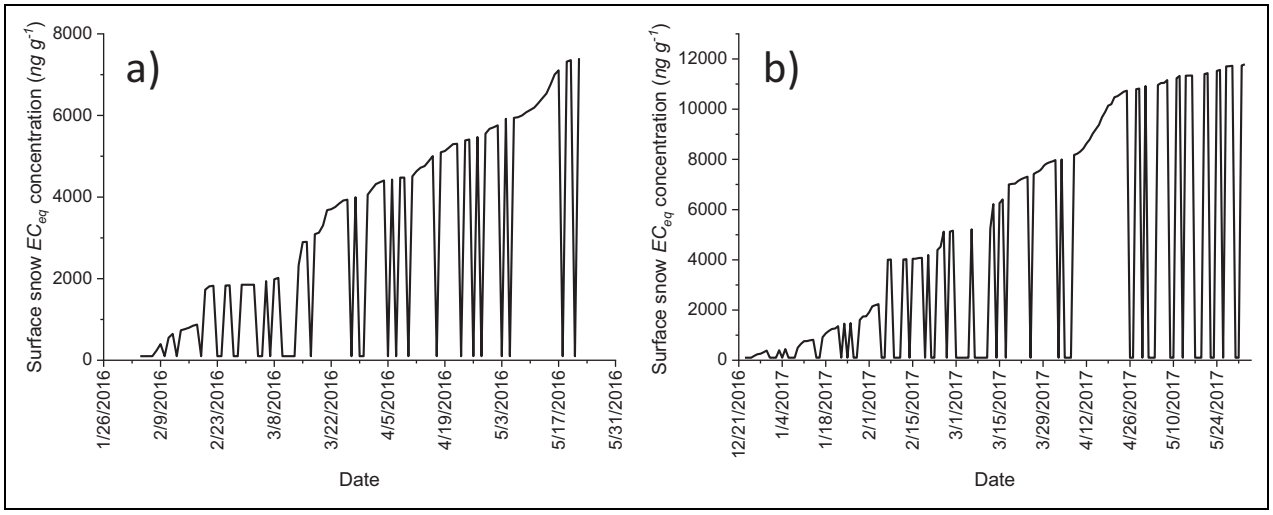

Figure 2. The estimated surface concentration of equivalent elemental carbon $[EC_{eq}]_{surf}$ based on Equations 1 and 2, applying the observed changes in snow depth and assuming the surface concentration of equivalent elemental carbon $[EC_{eq}]_{sp}$ of 100 ng g^{-1} and the parameter *d* of 4 mm for Season 1 (a) and Season 2 (b). The drops in surface concentration correspond to snow precipitation events. DOI: https://doi.org/10.1525/elementa.2021.000118.f2

where $[EC_{eq}]_{surf}$ is the snow surface concentration, n is the number of the day into the snow season, and $[EC_{eq}]_{sp}$ is the average snow precipitation concentration. In the second case, for a decreasing SD (SD^-), the accumulated deposition of LAP is equal to cumulative decrease in SD since the start of the seasonal snow cover multiplied by $[EC_{eq}]_{sp}$. This amount is assumed to be distributed over d at the surface. This is expressed as,

$$[EC_{eq}]_{surf\ n} = \left([EC_{eq}]_{sp} d + \sum_{i=1}^{n} SD_i^- \frac{\rho_{fs}}{\rho_w} [EC_{eq}]_{sp} \right) \Big/ d, \qquad (2)$$

where i is the number of the days since the start of the seasonal snow cover, SD_i^- is the absolute decrease in SD (mm per day) for day i, d is the characteristic depth of the surface layer (mm, SWE), ρ_{fs} and ρ_w are the density of fresh snow (100 kg m^{-3}; Helfricht et al., 2018) and liquid water (1,000 kg m^{-3}), respectively. In the third case, when the SD did not change from one day to another, the LAP content was set equal to the concentration of the previous day. Overall, these instances were few for both seasons.

The temporal evolution of $[EC_{eq}]_{surf}$ was controlled by the measured changes in SD, while its absolute value changed with the selection of $[EC_{eq}]_{sp}$ and d. As stated previously, our base case value for $[EC_{eq}]_{sp}$ is adopted from measurements by Svensson et al. (2021), but the value of d was semi-empirically adjusted as described in Section 2.5. As a result of this adjustment (in Section 2.5) a value of 4 mm was obtained and used in Equation 2. This is comparable to an average change in SD per day. The temporal evolution of $[EC_{eq}]_{surf}$ for the 2 seasonal snow cover periods, based on Equations 1 and 2 with $d = 4$ mm and $[EC_{eq}]_{sp} = 100$ ng g^{-1}, is depicted in **Figure 2a** and **b**. As can be seen in **Figure 2**, the estimated EC_{eq} concentration reach many thousands of nanograms per gram toward the end of the seasons because of the accumulation of EC in the surface layer. The dips in the concentrations correspond to episodes when the SD is increasing.

Note, that due to the trivial design of Equations 1 and 2, the vertical information concerning the where in the snowpack the LAP layer exist is not considered. This leads to the fluctuations in concentration, as seen in **Figure 2a** and **b**, to be over emphasized. Situations where this particularly influence the result is during a melt period that was preceded with a previous extensive melt and build-up of significant amounts of snow precipitation in between. During such periods, the concentration of LAP in the top layer will be overestimated.

2.2.2. Estimating snow grain effective radii, r_e

The second important variable in the formulation by Pedersen et al. (2015) is the snow grain effective radius since the albedo is very sensitive to the microphysical properties of the snow. For snow, the albedo decreases as the size of the grains increases (Warren and Wiscombe, 1980). Typically, snow grains undergo metamorphosis and become larger as snow ages and as the season progresses the albedo of snow decreases (e.g., Aoki et al., 2003). Several studies have used different approaches, including the temperature, to capture the metamorphism of snow and its effect on the albedo (e.g., Meinander et al., 2013, and references therein). Parameterizations used to match observations may for instance involve variations of summed daily maximum air temperatures since the last snow fall to capture the metamorphism of the snow over time (e.g., Winter, 1993; Brock et al., 2000). In numerous large-scale models such as CAM 3.0 (Collins et al., 2004), ECHAM5 (Roeckner et al., 2003; Roesch and Roeckner, 2006), or the ECWMF model (ECWMF, 2010) the snow albedo is linked with temperature either linearly or exponentially.

Downloaded from http://online.ucpress.edu/elementa/article-pdf/10/1/00118/716484/elementa.2021.00118.pdf by guest on 14 August 2024

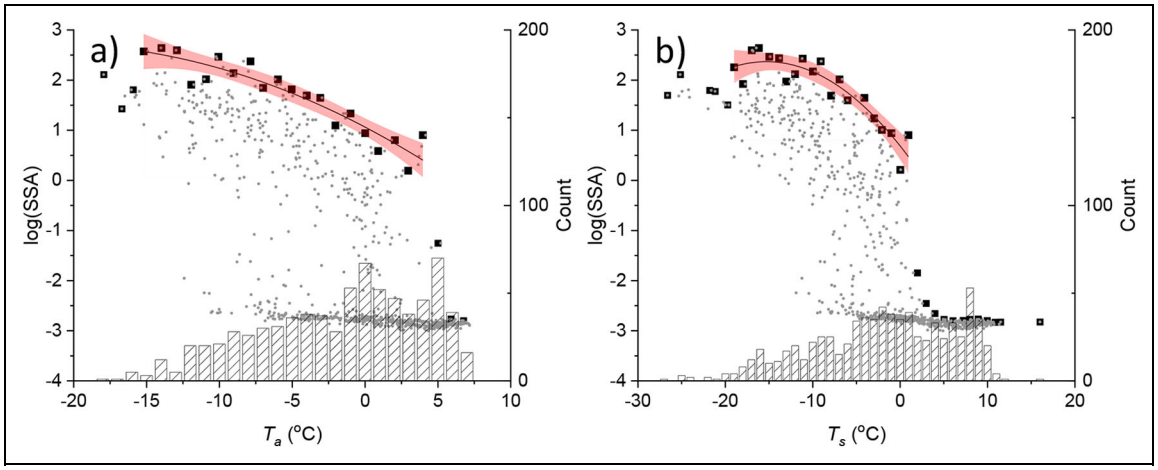

Figure 3. The parameterized specific surface area (log[SSA]) using Equation 4 as function of (a) air temperature and (b) the black body surface temperature. The gray dots are daily median values for all available data, including snow free summer conditions (note difference in *x* axis scale between graphs). Black squares are the maximum values in each 1° temperature bin. The solid black lines are fitted second degree polynomials to the maximum values. The 95% confidence range are marked with the red shaded areas. The histograms show the number of data points available in each temperature bin. The fitting was performed in the ranges −15.5°C to +4.5°C and −19.5°C to 1.5°C for the Seasons 1 and 2, respectively. DOI: https://doi.org/10.1525/elementa.2021.000118.f3

In this study, we will use the temperature as proxy for the grain size in surface snow and relate this to the most pristine snow. This is achieved by organizing all the albedo data as function of temperature in 1° bins (not only the 2 seasonal snow cover periods). We will explore the data using both the air temperature, T_a, and the black body temperature of the surface, T_s, which is given by the Stefan–Boltzmann law according to,

$$T_s = \sqrt[4]{\frac{\mathrm{LW}_u}{\varepsilon\sigma}}, \qquad (3)$$

where LW_u is the broad band long-wave radiated energy to the atmosphere (W m^{-2}), $\sigma = 5.67{\cdot}10^{-8}$ (W m^{-2}K^{-4}), and ε is the emissivity. For simplicity, unity is used for ε.

For each temperature bin, the maximum observed albedo is identified. The rational is that this condition represents the most pristine snow conditions observed for each temperature bin (i.e., with minimum influence from LAP). Each albedo value can be expressed as the specific surface area (SSA) of the surface snow using the parametric relation by Gardner and Sharp (2010) according to,

$$a_p = 1.48 - (10{*}\mathrm{SSA})^{-0.07}, \qquad (4)$$

where a_p is the albedo of pristine snow and SSA is given in ($m^2\ kg^{-1}$). Liquid water in snow may influence the albedo indirectly by enhancing r_e from filling the voids between the snow crystals during strong melt (Colbeck, 1979). This effect is not considered in our simplified approach. Scatterplots of log(SSA) as function of T_a and T_s are presented in **Figure 3a** and **b**, respectively.

The data in **Figure 3** present a consistent picture of decreasing maximum observed albedo (expressed as SSA) as function of temperature over a large temperature range. At low temperatures (below about $T_a = -15$ and $T_s = -19$), data deviates from the regression curve. However, only a limited number of measurements are available in this temperature range. At the other end of the temperature range, the obvious impact of strong snowmelt can be seen in the drop in albedo (expressed as SSA) at positive air temperatures and near zero for the surface temperature. To arrive at a useful relation between SSA and temperature, fitting of data were performed between −15.5 and +4.5 for air temperature and −19.5 and 1.5 for the surface temperature. The fact that surface temperature is above 0 can be explained by the assumed emissivity alone. The resulting fitted expressions are as follows:

$$\log(\mathrm{SSA}) = -3.51 \cdot 10^{-3} T_a^2 - 0.15 T_a + 1.06, \qquad (5)$$

$$\log(\mathrm{SSA}) = -7.18 \cdot 10^{-3} T_s^2 - 0.22 T_s + 0.69, \qquad (6)$$

and T_a and T_s are given in $^\circ C$.

These simple relations between SSA and temperature do not include the age of snow, which is used in several parameterizations (e.g., Adolph et al., 2016; Mimeau et al., 2019). That is, the information on the number of days since last snow fall is not part of the equation. Therefore, Equations 5 and 6 will result in the same SSA for a given temperature even if the snow fell at an earlier date at a different temperature. The systematic decrease in SSA with increasing temperature indicates that snow falling at a given temperature will adjust SSA as temperature increases. This corresponds to the growth of the snow grains. However, since our relations are based on maximum SSA values in each temperature bin, it is possible that some memory effects cause an overestimation of the SSA in a situation when the temperature increase after snow fall. In a similar way, decreasing temperatures would bias SSA toward lower values. With increasing amount of

Downloaded from http://online.ucpress.edu/elementa/article-pdf/10/1/00118/716484/elementa.2021.00118.pdf by guest on 14 August 2024

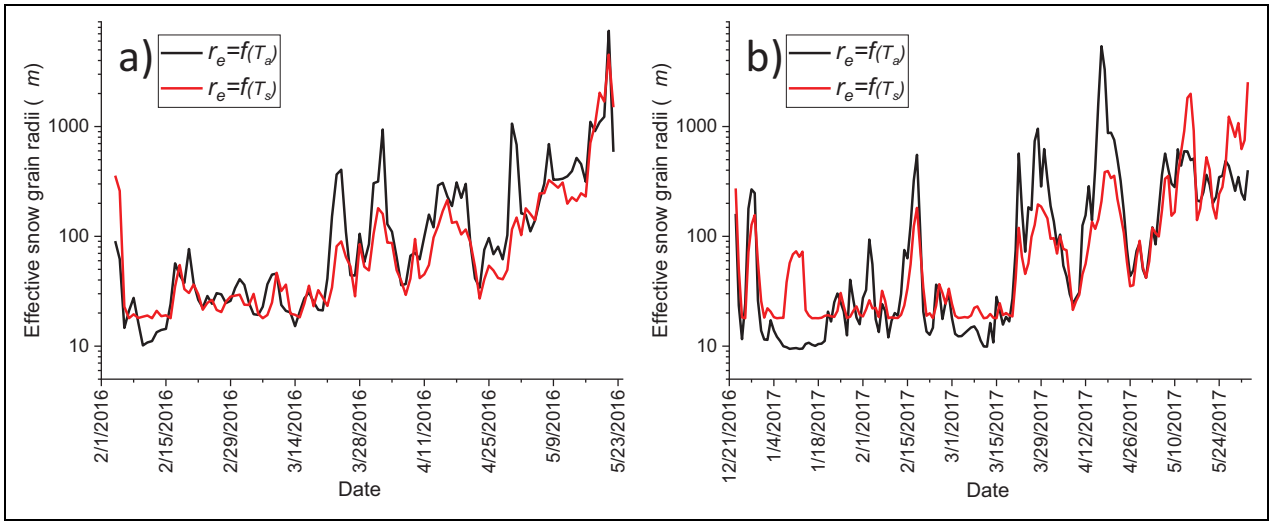

Figure 4. The estimated snow grain effective radii based on air temperature (black lines) and surface temperature (red lines) using Equations 5–7 for Season 1 (a) and Season 2 (b). DOI: https://doi.org/10.1525/elementa.2021.000118.f4

data in each temperature bin, the probability for masking such low bias is increasing. The drop in SSA seen at cold temperatures could be related to such conditions. The snow carries the memory of a lower SSA representative of warmer temperature. Due to the lack of data, this event will represent the maximum SSA values at cold temperatures. Overall, the diagnosed SSA based on the temperature in Equations 5 and 6 can be considered upper estimates. The sensitivity is, however, less than one might expect. As shown in Table S1, the effect from reducing SSA by 50% will cause a relative change in the estimated albedo of just below 10%.

The final step in deriving r_e is to estimate it from the ratio between volume and area of the grains according to,

$$r_e = \frac{3}{\rho_i \mathrm{SSA}}, \tag{7}$$

where ρ_i is the density of ice (910 kg m^{-3}) and SSA is the specific surface area of snow (m^2 kg^{-1}). Since SSA is related to temperature through Equations 5 and 6, r_e is also diagnosed by the temperature. The resulting temporal evolution of diagnosed r_e for the 2 seasons are shown in **Figure 4a** and **b**. As can be seen from **Figure 4**, r_e ranges from about 10 to 1,000 µm, generally increasing with time. This numerical exercise cannot be validated using our data set, but the resulting numerical values agree with previous studies (e.g., Painter et al., 2007; Adolph et al., 2016; Skiles and Painter, 2017) showing also similar seasonal trends.

2.3. Estimating the albedo reduction by LAP

The subsequent step is to estimate the albedo reduction based on $[\mathrm{EC_{eq}}]_{\mathrm{surf}}$ and r_e, derived in Sections 2.2.1 and 2.2.2. As mentioned above, we have chosen the empirical relation by Pedersen et al. (2015), which has the general form

$$y_\lambda = A - B\,x^C, \tag{8}$$

where y_λ is the spectrally dependent albedo reduction of pristine snow from the LAP expressed as EC_{eq}, λ is the wavelength, and A, B, and C are wavelength dependent constants provided for completeness in Supplement Table S2. The variable x is

$$x = \sqrt{[\mathrm{EC_{eq}}]_{\mathrm{surf}}}\, r_e, \tag{9}$$

where $[\mathrm{EC_{eq}}]_{\mathrm{surf}}$ is given in ng g^{-1} and r_e is given in µm. This parameterization is designed for $\mathrm{EC_{eq}}$ concentrations between 1 and 400 ng g^{-1}, but Svensson et al. (2016) has shown that it can be used with reasonable agreement also at significantly higher concentrations. Hence, the parameterization will also be used outside its original intended range in LAP.

The spectrally dependent y_λ, from Equation 8, is further weighted over the solar spectrum between 400 and 900 nm using table 1 of Hulstrom et al. (1985) to achieve the broad band scaling factor y_b. The albedo of the snow containing LAP was then estimated by scaling a_p from Equation 4 with y_b,

$$a = a_p y_b. \tag{10}$$

This does not consider the influence from the underlaying surface that potentially becomes progressively larger as the SD decreases. This behavior is further elaborated in the subsequent section.

2.4. Estimating the influence from ground albedo on measurements and adjusting characteristics depth parameter d

As outlined in Section 2.2.1, the parameter d is important in scaling the surface concentration of $\mathrm{EC_{eq}}$. Our approach to find the most suitable value for d is to change its value in an attempt to minimize the difference between the observed albedo (a_{obs}) and the derived albedo from Equation 10. The difference is expressed as the sum of

Downloaded from http://online.ucpress.edu/elementa/article-pdf/10/1/00118/716484/elementa.2021.00118.pdf by guest on 14 August 2024

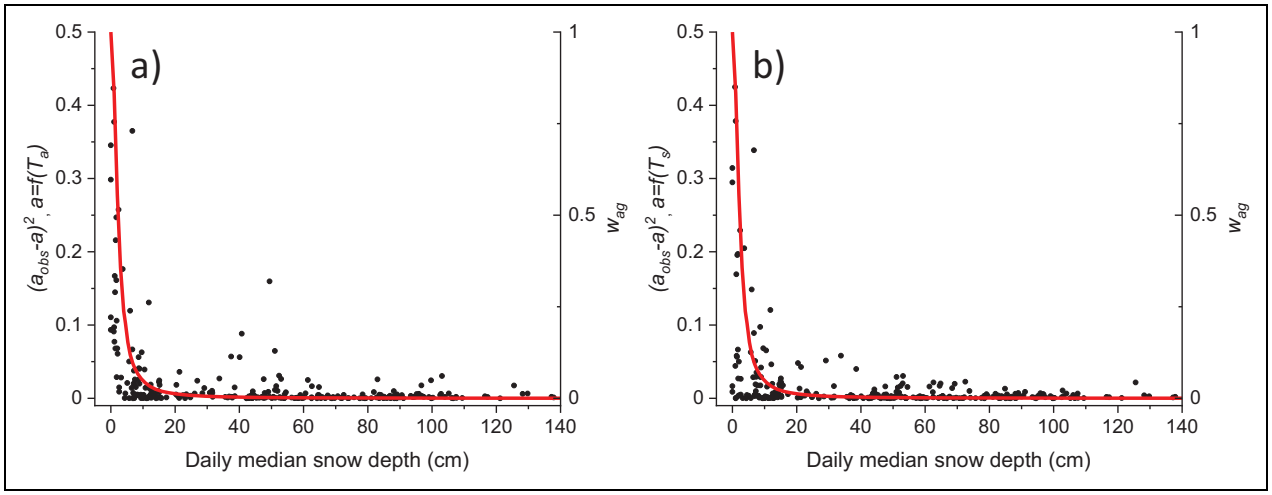

Figure 5. Dots are the squared differences between observed albedo and the estimated albedo for both seasons using snow depth (SD) changes and the air temperature (a), or surface temperature (b), as variables. For these calculations, a characteristic depth of surface snow (d) value of 4 mm was used. The red line in each subplot is the weighting factor between a and a_g as a function of snow depth w_{ag}, see text for details. DOI: https://doi.org/10.1525/elementa.2021.000118.f5

$(a_{obs} - a)^2$. The differences were calculated using different choices of d and the 2 temperatures T_a and T_s, respectively.

However, the influence from the underlaying surface on the total snow albedo must first be considered. For a thin snow layer, the absorption at ground will lower the overall albedo, and at some point the snow will become patchy, with rocks starting to protrude through the surface of the snow resulting in a lower average albedo over the footprint of the sensor. To investigate this effect, $\sum (a_{obs} - a)^2$ is plotted as a function of SD, where a is estimated using $d = 4$ mm, and both data sets using Equations 5 and 6 (T_a or T_s) are combined. The data are presented in **Figure 5**, where $\sum (a_{obs} - a)^2$ is presented using an arbitrary unit.

At SDs greater than about 50 cm, the deviations remain relatively small in **Figure 5**. At SDs less than about 20 cm, there is an apparent increase in the deviations with decreasing SD. Based on these results, only data for SD > 55 cm are used to determine the best value for the parameter d. The value of 55 cm is chosen to safely exclude any influence from the ground surface or rocks and to exclude the outliers around 50 cm visible in **Figure 5**. It is larger than the value of 30 cm used, for example, by Reveillet et al. (2021) to define snow cover in their modeling study.

Using the subset of the data for SD > 55 cm, $\sum (a_{obs} - a)^2$ is calculated for different values of d. The result is presented in **Figure 6**, where an arbitrary unit is used for the deviations.

As d increases from 0.5 to 4 mm, the deviations clearly decrease and the agreement between observed and derived albedo improves. From a minimum value around 4 mm, the deviations gradually increase, which indicates that the agreement becomes less satisfactory. Hence, a d value of 4 mm was selected since it results in the smallest deviation between observed and estimated albedo. This parameter can be viewed as a numerical fix to other

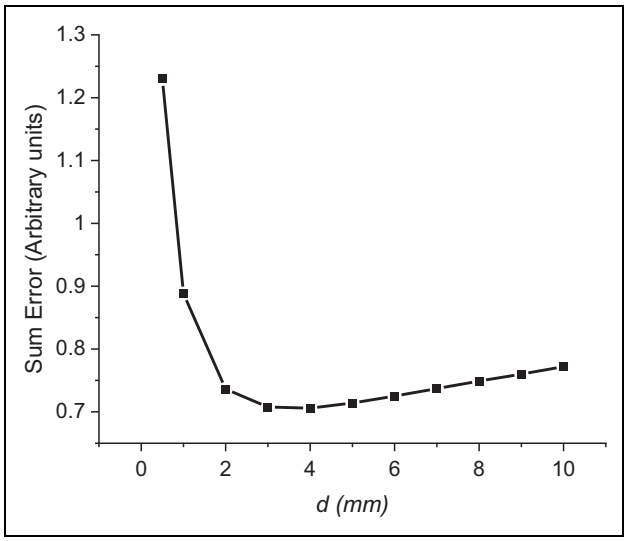

Figure 6. Sum of errors as function of the characteristic depth of surface snow (d). Errors, $(a_{obs} - a)^2$, are summed up for both seasons and both temperature parameterizations of Equations 5 and 6. Only data with snow depth >55 cm are included. DOI: https://doi.org/10.1525/elementa.2021.000118.f6

shortcomings in the assumptions made above, but a physical interpretation of d is that it represents some e-folding thickness of the surface layer, where LAP accumulates and interacts with radiation. Since d is expressed as mm SWE, the actual geometric thickness will depend on snow density. In its physical sense, d is not a constant but depends on the optical properties of the surface snow as well. For instance, a more transparent snow will allow the light to penetrate deeper for the same amount of SWE. This dependence is included to some extent in Equation 9, where it is shown that the absorption efficiency by LAP is scaled with the grain size. In a more detailed model

Downloaded from http://online.ucpress.edu/elementa/article-pdf/10/1/00118/716484/elementa.2021.00118.pdf by guest on 14 August 2024

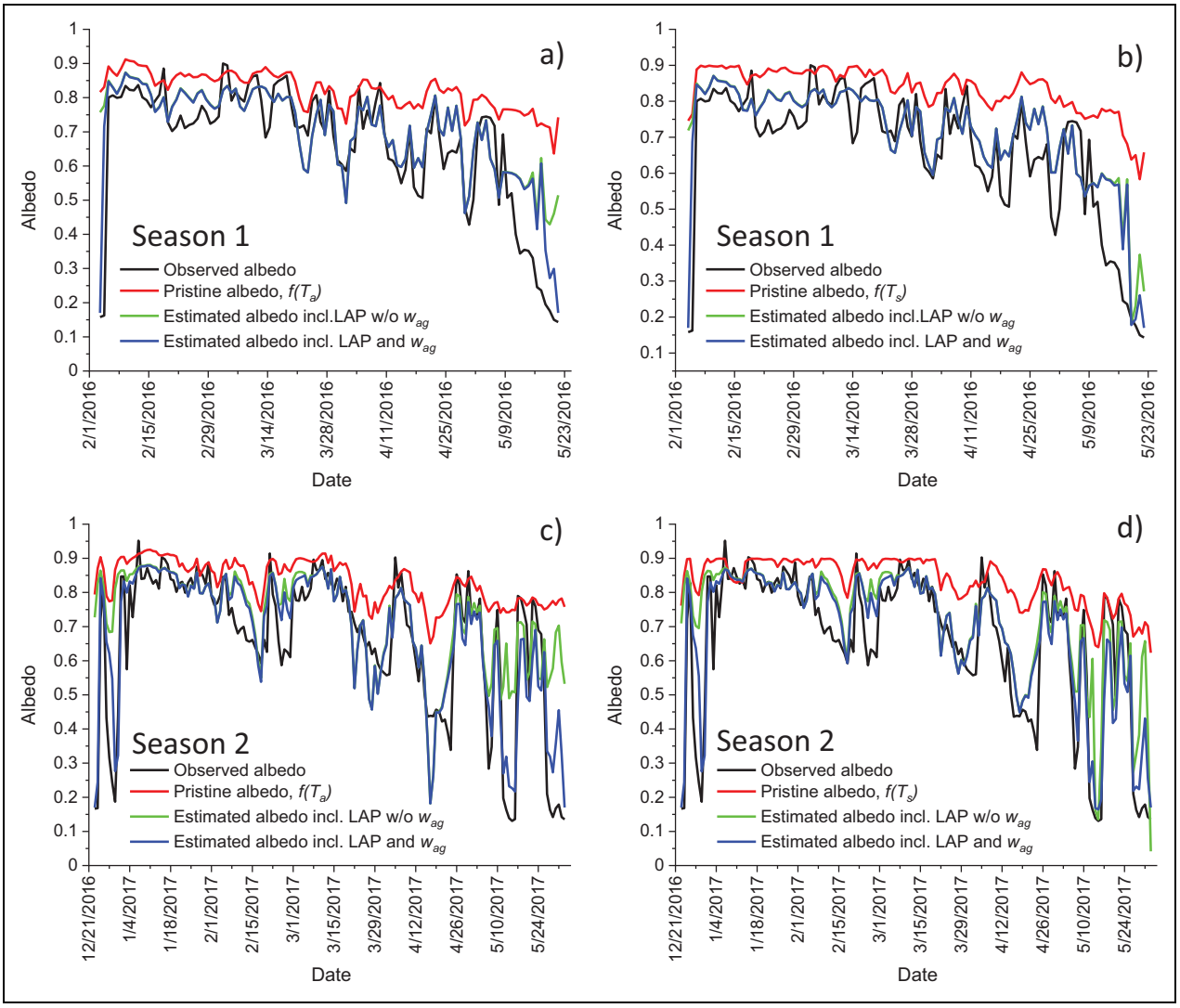

Figure 7. The observed albedo and emulated albedo using T_a or T_s with and without light-absorbing particles (LAP) and the influence from the underlying ground surface. Season 1 is presented in panel (a) and (b) using T_a and T_s, respectively. Season 2 is presented in panel (c) and (d) utilizing T_a and T_s, respectively. DOI: https://doi.org/10.1525/elementa.2021.000118.f7

framework (e.g., Niwano et al., 2021), where the LAP has a more realistic vertical distribution in the snowpack, the estimated top layer and its LAP concentration will be less than what is assumed here. Likewise, such a framework would also have a different d, and is likely to be greater than 4 mm to fully encompass the optically active surface snow layers. In the interest of keeping our approach simple, the vertical information of LAP is not maintained.

To accommodate the obvious influence from the ground albedo (a_g) for small SD, a simple mixing rule was introduced. The snow free ground albedo, a_g, taken as 0.17 (based on observed albedo of bare ground before and after the snow seasons, **Figure 1**), is weighted with a using a factor $w_{a_g} = f(\mathrm{SD})$. SD is given in cm. This function gives a weight of one at SD = 0 cm and decreases toward zero as SD increases. The functional dependence of f(SD) is $1/\left(1+\frac{\mathrm{SD}^2}{5}\right)$ and presented in **Figure 5**. As will be evident below (cf., **Figure 7**), the influence from a_g to the total albedo is only important at the very start and toward the end of the seasons. As this weighting function only serves to blend the transition between the snow albedo and a_g at small SD, no particular effort to adjust this model or motivate its shape was performed. The final estimated albedo including the influence from the ground albedo is calculated as

$$\text{albedo} = a(1 - w_{a_g}) + a_g w_{a_g}. \quad (11)$$

3. Comparison between observations and derived albedo and absorbed solar energy

3.1. Observed versus parameterized albedo

The time series of observed albedo are compared to different parameterized albedos for each season and temperature relation (Equations 5 and 6) in **Figure 7a–d**. In each figure, the observed albedo is compared with the pristine snow albedo (a_p, based on Equations 4 and 5 or 6), and the estimated snow albedo containing LAP with and without the effect from the ground albedo (Equations 10 and 11).

Downloaded from http://online.ucpress.edu/elementa/article-pdf/10/1/00118/716484/elementa.2021.00118.pdf by guest on 14 August 2024

As expected, a_p (depicted by red line) is generally higher than the observed albedo (black line). There are a few occasions where the observed albedo exceeds a_p, and the reason is apparent from **Figure 3**, where about half of the maximum data points are above the fitted line. When calculating a_p using either T_a or T_s, it is noticeable that the results are very similar, although not identical. Nevertheless, a_p does capture the observed seasonal albedo progression well, decreasing from about 0.9 in the beginning of the seasons to about 0.75 toward the end of the seasons. Effectively, this is very similar to albedo models based on temperature and number of days since last snow fall such as proposed by Adolph et al. (2016). The Pearson correlation, r^2, between the observed albedo and a_p (only derived from temperature in this study via Equations 4, 5, and 6) is 0.5, which is comparable to the 0.52 reported by Adolph et al. (2016) that includes the snow fall information.

Taking LAP into account (green line, **Figure 7**), for the base case of $[EC_{eq}]_{sp} = 100$ ng g^{-1} and $d = 4$ mm, the agreement between observed and derived albedo improves. The difference between pristine albedo (the red line) and the estimated albedo excluding ground albedo effect (the green line, mostly covered by the blue line) represents the albedo reduction due to LAP. The difference between the green and blue lines represents the effect from ground albedo. This difference increases over time with intermittent recoveries (smaller differences) as associated with new snow events. The modeled and observed albedo agree better by considering the influence by the ground albedo (blue line, which is visible especially at either end of the seasons as intended with Equation 11. However, there are also periods during the seasons where the snow albedo is reduced significantly only due to accumulated LAP on the surface. These periods are visible from the relatively large difference between red and blue lines, without contribution from the underlaying ground albedo (green line). In April, the albedo can be as low as ca. 0.4, from the combined effect of snow grain size and LAP. The selection of the temperature between ambient (T_a) and (T_s) does not impact the final result (**Figure 7a** vs. **7b** and **Figure 7c** vs. **7d**). Using T_a, however, results in spurious occasions of low albedo not supported by observations. These occasions were linked to episodes of warm air temperatures exaggerating the diagnosed r_e.

Scatter plots of the parameterized and observed albedo are presented in **Figure 8**, including linear regressions. As already evident in **Figure 7**, using either T_a or T_s give very similar results. The regressions coefficients are 0.75 and 0.76, the intercepts are 0.19 and 0.20, and the Pearson correlations, r^2, are 0.76 and 0.79 for air and surface temperatures, respectively. Hence, using T_s as the proxy for the pristine albedo and r_e, result in only a marginally closer agreement to the observed albedos. The 2 seasons together represent almost 9 months of daily albedo data parameterized using only temperature and changes in SD as the time dependent variables. The regression slopes suggest a bias overestimating the lower values, which probably is related to the remaining influence from

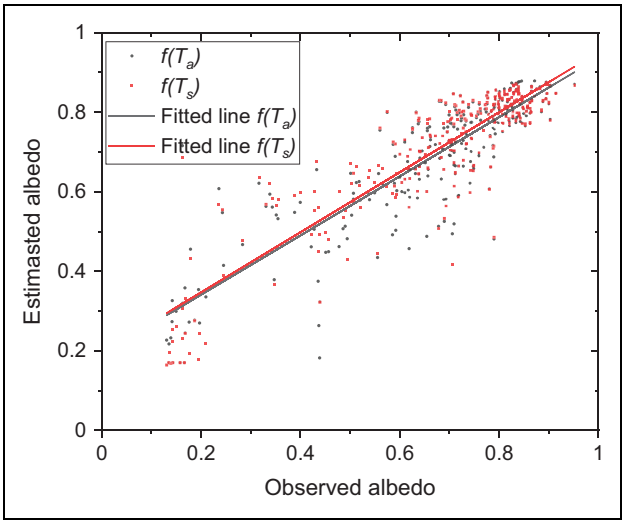

Figure 8. Scatterplot showing the relation between estimated and observed albedo for both seasons combined. Black dots show the estimated values using air temperature as proxy for r_e. Red dots show data for values using the surface temperature as proxy for r_e. The fitted lines, depicted in corresponding colors, have slopes of 0.75 and 0.76, and intercepts of 0.19 and 0.20, respectively. The Pearson correlations, r^2, are 0.76 and 0.79 for air and surface temperature, respectively. Estimated albedo was calculated for average snow precipitation concentration of $[EC_{eq}]_{sp} = 100$ ng g^{-1}.
DOI: https://doi.org/10.1525/elementa.2021.000118.f8

ground albedo of 0.17. It is worth noting that the data points are not distributed evenly over the domain from about 0.2 to 0.9, and that there is a seasonal trend in albedo. Therefore, the regression analysis offers a limited perspective, and it is more interesting to compare the integrated solar energy absorbed at the end of the season based on the observed albedo and for different LAP scenarios. This is presented in Section 3.2.

3.2. The relation between LAP, albedo, and absorbed solar energy

The analysis above shows that much of the variability in snow albedo for a seasonal snow cover can be reproduced based on a few assumptions and using only 2 observed parameters, temperature and SD. These albedo variations are significant due to their impact on the total absorbed incoming short wave radiation at the end of the season. To quantify this impact, the integrated absorbed solar energy was compared for the observed albedo in a range of $[EC_{eq}]_{sp}$ values. Despite the fact that T_s gave slightly better agreement between the observed and estimated albedos, we will use only T_a as our temperature variable in the subsequent analysis. This is because the 2 data sets are very similar, but also because T_a is a more basic variable and readily available, compared to the black body temperature. The results are presented in **Figure 9 a–b**, as cumulative plots, and the ratio and absolute difference between the observations and estimated albedo using our base case scenario. At the end of the seasons, the base case

Downloaded from http://online.ucpress.edu/elementa/article-pdf/10/1/00118/716484/elementa.2021.00118.pdf by guest on 14 August 2024

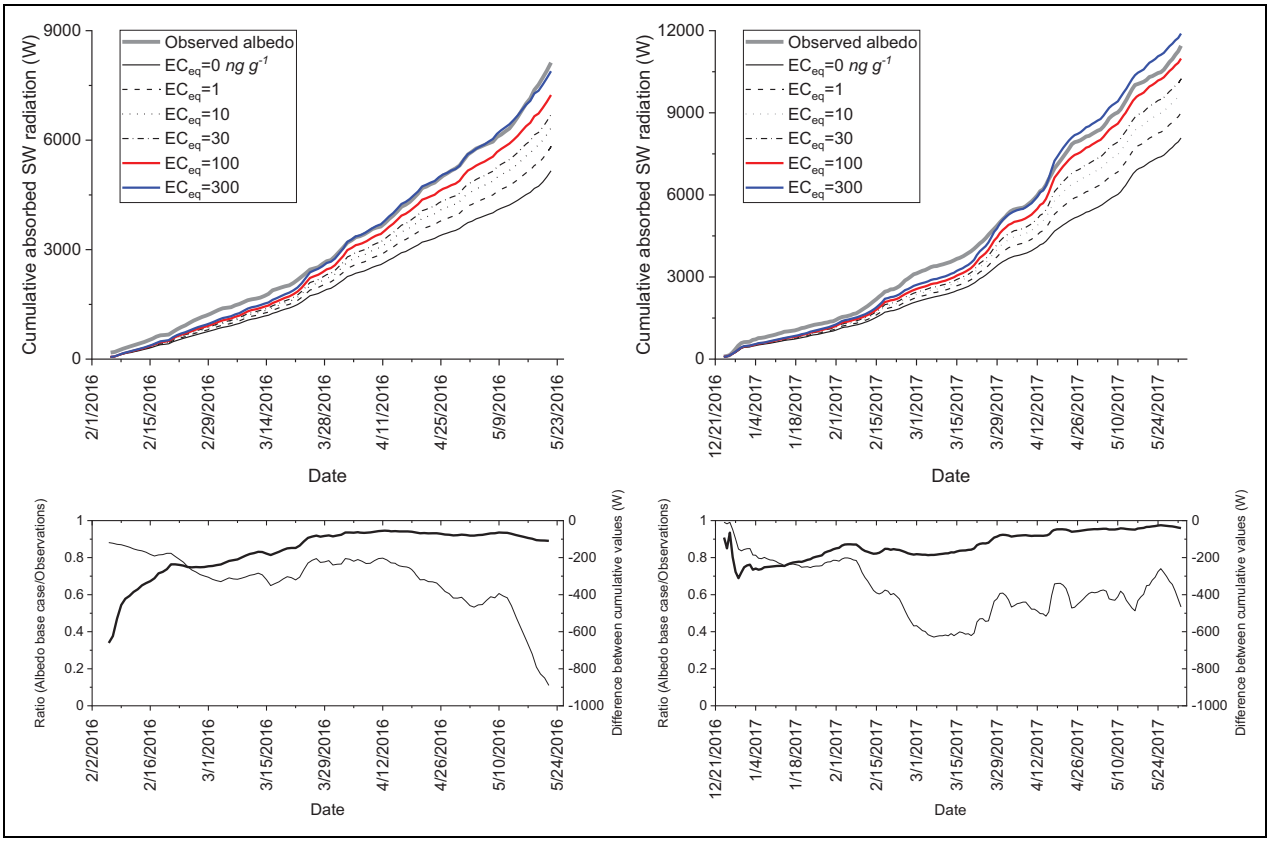

Figure 9. Upper panels present the cumulative absorbed short wave (SW) radiation based on the observed albedo and estimates using different light-absorbing particles (LAP) concentrations in snow precipitation for Seasons 1 (a) and 2 (b). The base case is depicted by the red line. Lower panels present the ratio (thicker line) between the observations (thick black line in upper panel) and the base case (red line in upper panel), as well as the cumulative difference (thinner line) between observations and base case for the respective seasons. DOI: https://doi.org/10.1525/elementa.2021.000118.f9

integrated energy agrees within 11% for Season 1 and 4% for Season 2. For both seasons, the ratios lag behind from the start, but in the second half of the seasons, the ratios have recovered to be about 10% from the observed values. This suggests that the absorbed energy is generally underestimated at the start of the seasons, which is essentially compensated for by generally overestimating the absorption during the later part of the seasons.

From the different $[EC_{eq}]_{sp}$scenarios in **Figure 9**, it is evident that the integrated SW radiation is rather insensitive to variations in LAP in the beginning of the seasons. This suggests that our overestimation of the albedo is linked to parametric relations in Equations 4 and 5 and the microphysical properties of pristine snow, as discussed in Section 2.3. The reason for underestimating the albedo can of course be related to the choice of $[EC_{eq}]_{sp}$ and value of d, but also that the parametric relation by Pedersen et al. (2015) is extrapolated to large LAP surface concentrations.

Despite systematic and partly compensating effects, the overall agreement between the cumulative absorbed SW energy and our base case scenario agrees well, as seen in **Figure 9**. We conclude from this that using an average LAP concentration in snow precipitation and the simple surface aggregation based on SD changes, the key features in the temporal evolution of surface snow albedo are captured. By comparing different LAP concentrations to $[EC_{eq}]_{sp} = 0$, the enhancement in integrated absorbed SW radiation can be calculated as a function of $[EC_{eq}]_{sp}$. Integrated energies were calculated for 0, 0.1, 0.3, 1, 3, 10, 100, and 300 ng g^{-1}. This comparison is presented in **Figure 10** indicating how much more energy is absorbed as function of $[EC_{eq}]_{sp}$compared to $[EC_{eq}]_{sp} = 0$. Despite different duration (106 vs. 159 days) and precipitation amounts (290 vs. 460 mm), the 2 seasons present the same relative enhancement for a given $[EC_{eq}]_{sp}$. For our base case example of 100 ng g^{-1}, both seasons show an extra absorption of solar energy of 40% and 36%, respectively.

The fitted expressions to this data (in **Figure 10**), $y = 0.128[EC_{eq}]_{sp}^{0.249}$ for Season 1 and $y = 0.114[EC_{eq}]_{sp}^{0.249}$ for Season 2, provide another important insight with respect to the sensitivity of absorbed energy due to changes in LAP. If the LAP content is changed by a factor of 2, the extra energy absorbed by the snow is changed by a factor of 2^b, where b is the exponent from the fitted expressions. For both seasons this is around 20%. In the following Section 3.3, we illustrate the implication of this result on the duration of a melt period using a numerical example.

Downloaded from http://online.ucpress.edu/elementa/article-pdf/10/1/00118/716484/elementa.2021.00118.pdf by guest on 14 August 2024

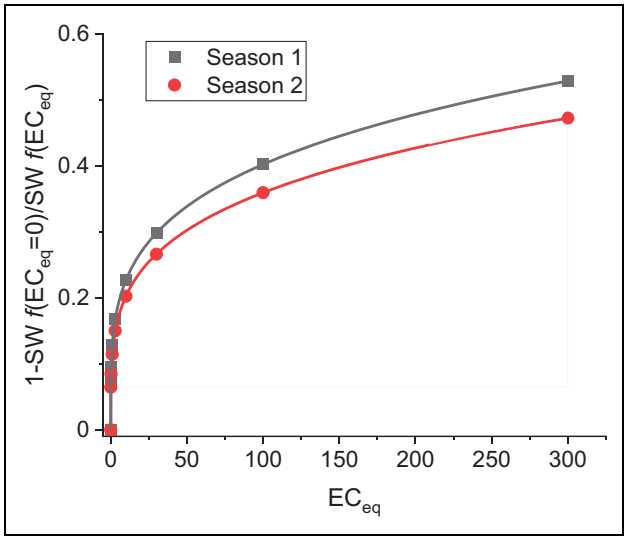

Figure 10. Relative enhancement of absorbed short wave (SW) as function of ECeq concentration in snow precipitation for Season 1 (black) and Season 2 (red). The solid lines represent fitted power relations mentioned in the text. DOI: https://doi.org/10.1525/elementa.2021.000118.f10

3.3. Doubling the average LAP concentration in snow precipitation: Implications using a numerical example

All of the accumulated absorbed SW radiation energy is not available to melt snow since a fraction of the energy is radiated back to the atmosphere as long wave thermal radiation, and a fraction is exchanged through latent and sensible heat fluxes (partly compensating each other). However, if one assumes that processes that redistributes this absorbed energy, not used to ablate snow, can be approximated by proportionality, then the melt rate will be proportional to the changes in energy flux. For instance, due to a lowering of the albedo as consequence of LAP deposited in surface snow. Hence, as a first approximation, if one unit of energy is required to melt a given amount of snow in one day, double the amount of energy available will melt the same amount of snow in half the time.

For this example, we picked a melt period of 30 days for snow unaffected by LAP. The normalized amount of absorbed SW radiation required to arrive at 30 days is unity. This example may represent many different conditions, such as different geographical locations and amount of snow. Hence, without the influence of LAP, the melt period is simply 30 days divided by 1.

To include the effect from LAP, we use the results from the base case scenario, using an average snow precipitation EC_{eq} concentration of 100 ng g^{-1}. The accumulated absorbed SW radiation relative enhancement over the seasons were 40% and 36%, respectively. For the numerical example, we chose a value of 38% which is in between the 2 observed values. Assuming proportionality as described above, the length of the melt period including the effect from LAP is given by

$$\text{Length of melt period} = \frac{30}{(1+0.38)}, \qquad (12)$$

which is 21.7 days. The effect from including LAP (corresponding to our base case) therefore leads to a reduction in the melt period of just above 8 days.

The final step is to change the average concentration of LAP by a factor of 2 and calculate the change in the length of the melt period. From **Figure 9**, the curve fittings provided the same relation for the 2 seasons, namely, a factor 2^b, where $b = 0.246$. That means that each change in LAP by a factor of 2, corresponds to a change in the relative absorbed amount of SW energy by 18.8%. The length of the melt period doubling the base case concentration is given by,

$$\text{Length of melt period} = \frac{30}{(1+0.38\cdot 1.19)}, \qquad (13)$$

which is 20.7 days. The effect from doubling LAP (corresponding to our base case) leads to an additional reduction of merely 1 day.

Although the melt-out date (MOD) can be shifted significantly due to LAP, it is rather insensitive to relatively large changes in the average deposition. This is because already small LAP concentrations significantly affect the albedo. According to **Figure 10**, a LAP concentration of as little as 1 ng g^{-1} can potentially change the absorbed SW radiation by about 10%, which is the effect from the accumulation at the surface during melt (cf. **Figure 9**). On the other hand, but for the same reason, larger LAP concentrations will saturate, which is given by the square root dependence in Equation 9. **Figure 10** represents the increased energy due to the reduction in albedo over the whole season including the surface enhancement of LAP during melt. Higher concentration will of course lead to earlier MOD, but the sensitivity decreases with increased averaged LAP concentration in snow precipitation.

4. Summary and conclusion

A simple method to estimate changes in snow surface albedo was presented and compared to observations conducted during 2 seasons at a high-altitude site in Central Himalaya, India. The approach is based on key assumptions about the constant wet deposition of LAP, diagnosed temperature dependent snow grain size, and the albedo reduction due to EC_{eq} following the parameterization by Pedersen et al. (2015). It is assumed that EC and MD have an equal contribution to the LAP in terms of absorption based on the observations in Svensson et al. (2021) and that the increase in LAP concentration in surface snow is a function of the constant concentration in snow precipitation multiplied by the reduction in SD. The latter relation mimics the aggregation of LAP in the surface layer as snow ablates. The effective radii of the snow grains r_e were estimated based on the fitted relationship between albedo, SSA, and r_e. The AWS data were grouped into 1° temperature bins and a function between air temperature and the maximum observed albedo (expressed as log(SSA)) for each bin was fitted. The derived LAP concentration in surface snow expressed as EC_{eq} and the diagnosed r_e are the final variables used as inputs to parameterize the albedo reduction due to LAP. To

Downloaded from http://online.ucpress.edu/elementa/article-pdf/10/1/00118/716484/elementa.2021.00118.pdf by guest on 14 August 2024

diagnose r_e, the black body surface temperature was tested as an alternative parameter to estimate r_e, but it only marginally improved the agreement between observed and estimated albedo. Hence, the only time-dependent variables that are required to estimate snow surface albedo in our simplified model is air temperature and the SD.

In our base case simulation, we used an estimated EC_{eq} = 100 ng g^{-1} in snow precipitation. Comparison of the observed daily median albedo and the parameterized albedo using the base case yielded a linear regression slope of 0.75 and a Person correlation coefficient, r^2 = 0.76, using air temperature as proxy for r_e. However, comparing the integrated amount of SW radiation absorbed over the season using observed albedo versus base case albedo resulted in rather small differences of 11% and 4% at the end of Season 1 and 2, respectively.

The variability in albedo is essentially captured and reproduced over the 2 seasons tested even with the simplistic approach described in this study. Encouraged by these results, the enhanced absorbed SW radiation at the end of the seasons were investigated using a range of constant LAP concentration in snow precipitation from 0 to 300 ng g^{-1}. The calculated absorbed SW energy as function of LAP concentration was compared to pristine snow, $[EC_{eq}]_{sp}$ = 0. The fitted fractional short wave enhancements by LAP were very similar for the 2 seasons. For Season 1, we obtained a parametrization for the enhancement $y = 0.128[EC_{eq}]_{sp}^{0.249}$and for Season 2 $y = 0.114[EC_{eq}]_{sp}^{0.249}$. The power law exponent indicates that any given proportional change in $[EC_{eq}]_{sp}$ will result in the same proportional change in enhanced SW for different absolute values of $[EC_{eq}]_{sp}$ >0. Hence, a factor of 2 changes in $[EC_{eq}]_{sp}$ will change the enhanced absorbed SW at the end of the season by $2^{0.249}$ = 1.188, or about 19%. This led to the conclusion that the changes in the absorbed SW radiation are not so sensitive to even relatively large changes in average LAP deposition. However, the influence by LAP is visible already at low concentrations. A factor of 100 less LAP would still lead to the absorption of about one third of the additionally absorbed energy due to the presence of LAP. Note that as long as the absorbing constituent is expressed as EC_{eq}, the results do not depend on what the LAP is composed of. A doubling will lead to the same absorbed extra energy. However, it also requires that the constituent follows the simple rule of staying near the surface layer as the snow ablates, which is probably not the case if the LAP is water soluble.

The motivation of this work has been to simplify the complex evolution of snow albedo with the influence of LAP specifically, and it has proven to deliver useful insights. Future work could possibly be improved by maintaining the vertical distribution of LAP in a more realistic manner throughout the snowpack. The basis for this work is the assumption that deposition of LAP can be described by a constant mixing ratio in snow precipitation, but EC and MD may be either wet or dry deposited separately and in variable amounts (e.g., as plumes). Preliminary investigations (out of scope of this study) using the same framework as presented in this study were conducted using variable deposition of EC and MD. Instead of a constant value, deposition was based on a combination of assumed probability functions separately for EC and MD. The results suggest that, as long as the total amount of LAP deposited during the season remains the same, the final amount of accumulated extra energy is not significantly dependent on the details about the timing of the deposition. This can be one contributing circumstance that explains why our simple approach perform relatively well compared to observations for both seasons. However, this topic requires a dedicated study. Further, the work could be extended to answer the question: What is the contribution to the number of days with snowmelt from a given change of LAP in the seasonal snow for the study region? Finally, clearly this simple approach performed well in estimating the snow surface albedo for 2 seasons at one location, using a minimum of input data. It would be of great interest to improve our approach and to test it for other geographical areas, as well as over longer timescales.

Data accessibility statement

Data is accessible through the Finnish Meteorological Institute open access database (http://doi.org/10.23728/fmi-b2share.9b887cbe454d42b5b9dd50127b7eaf1f).

Supplemental files

The supplemental files for this article can be found as follows:

List of acronyms used in the study and their units (where applicable).

Figure S1. Flow chart of the methodology described in Section 2.

Figure S2. AWS data from the two seasons.

Table S1. Albedo sensitivity to a 50% reduction in SSA.

Table S2. Parametric relation proposed by Pedersen et al. (2015).

Funding

This work has been supported by the Academy of Finland project: Absorbing Aerosols and Fate of Indian Glaciers (AAFIG; project number 268004), and the Academy of Finland consortiums: "Novel Assessment of Black Carbon in the Eurasian Arctic: From Historical Concentrations and Sources to Future Climate Impacts" (NABCEA project number 296302), "Black and Brown Carbon in the Atmosphere and the Cryosphere" (BBrCAC project number 341271), and the Academy of Finland Flagship (Grant No. 337552). J St. is part of the Bolin Centre for Climate Research, and acknowledges the Swedish Research Council grant 2017-03758. J Sv. acknowledges support from the 2 foundations Maj and Tor Nessling and Oskar Huttunen, as well as the invited scientist grant from the University Grenoble Alpes.

Competing interests

The authors have declared that no competing interests exist.

Downloaded from http://online.ucpress.edu/elementa/article-pdf/10/1/00118/716484/elementa.2021.00118.pdf by guest on 14 August 2024

Author contributions

Contributed to conception and design: JSt, JSv, HL, AH.

Contributed to acquisition of data: JSv, HH, EA, NBD, RH, VPS, ST, HL.

Contributed to analysis and interpretation of data: JSt, JSv, EA, OM, H-WJ, ML, AH.

Drafted and/or revised the article: JSt, JSv, EA, OM, H-WJ, ML.

References

Adolph, AC, **Albert, MR**, **Lazarcik, J**, **Dibb, JE**, **Amante, JM**, **Price, A**. 2016. Dominance of grain size impacts on seasonal snow albedo at open sites in New Hampshire. *Journal of Geophysical Research: Atmospheres* **122**: 121–139. DOI: https://dx.doi.org/10.1002/2016JD025362.

Aoki, T, **Hachikubo, A**, **Hori, M**. 2003. Effects of snow physical parameters on shortwave broadband albedos. *Journal of Geophysical Research: Atmospheres* **108**: 4616. DOI: https://dx.doi.org/10.1029/2003JD003506.

Armstrong, RL, **Rittger, K**, **Brodzik, MJ**, **Racoviteanu, A**, **Barrett, AP**, **Khalsa, SJS**, **Raup, B**, **Hill, AF**, **Khan, AL**, **Wilson, AM**, **Kayastha, RB**, **Fetterer, F**, **Armstrong, B**. 2019. Runoff from glacier ice and seasonal snow in high Asia: Separating melt water sources in river flow. *Regional Environmental Change* **19**: 1249–1261. DOI: https://dx.doi.org/10.1007/s10113-018-1429-0.

Bonasoni, P, **Laj, P**, **Marinoni, A**, **Sprenger, M**, **Angelini, F**, **Arduini, J**, **Bonafè, U**, **Calzolari, F**, **Colombo, T**, **Decesari, S**, **Di Biagio, C**, **di Sarra, AG**, **Evangelisti, F**, **Duchi, R**, **Facchini, MC**, **Fuzzi, S**, **Gobbi, GP**, **Maione, M**, **Panday, A**, **Roccato, F**, **Sellegri, K**, **Venzac, H**, **Verza, GP**, **Villani, P**, **Vuillermoz, E**, **Cristofanelli, P**. 2010. Atmospheric brown clouds in the Himalayas: First two years of continuous observations at the Nepal Climate Observatory-Pyramid (5079 m). *Atmospheric Chemical Physics* **10**: 7515–7531. DOI: https://dx.doi.org/10.5194/acp-10-7515-2010.

Brock, BW, **Willis, IC**, **Sharp, MJ**. 2000. Measurement and parameterization of albedo variations at Haut Glacier d'Arolla, Switzerland. *Journal of Glaciology* **46**: 675–688.

Colbeck, SC. 1979. Grain clusters in wet snow. *Journal of Colloid and Interface Science* **72**(3): 371–384. DOI: https://dx.doi.org/10.1016/0021-9797(79)90340-0.

Collins, WD, **Rasch, PJ**, **Boville, BA**, **Hack, JJ**, **McCaa, JR**, **Williamson, DL**, **Kiehl, J**, **Briegleb, B**, **Bitz, C**, **Lin, S-J**, **Zhang, M**, **Dai, Y**. 2004 June. Description of the NCAR Community Atmosphere Model (CAM 3.0), NCAR/TN-464+STR NCAR TECHNICAL NOTE. Available at http://www.cesm.ucar.edu/models/atmcam/docs/description/node35.html.

Cuffey, K, **Paterson, WSB**. 2010. *The physics of glaciers*. Burlington, MA: Elsevier, Butterworth-Heineman.

Doherty, SJ, **Grenfell, TC**, **Forsström, S**, **Hegg, DL**, **Brandt, RE**, **Warren, SG**. 2013. Observed vertical redistribution of black carbon and other insoluble light-absorbing particles in melting snow. *Journal of Geophysical Research: Atmospheres* **118**: 1–17. DOI: https://dx.doi.org/10.1002/jgrd.50235.

ECWMF. 2010. The European Centre for Medium-Range Weather Forecasts, The ECMWF Integrated Forecast System (IFS), IFS documentation CY25r1, operational on 9 April 2002, Eq. 7.29. Available at http://www.ecmwf.int/research/ifsdocs/CY25r1/Physics/Physics-08-05.htm.

Emerson, EW, **Katich, JM**, **Schwarz, JP**, **McMeeking, GR**, **Farmer, DK**. 2018. Direct measurements of dry and wet deposition of black carbon over a grassland. *Journal of Geophysical Research: Atmospheres* **123**(21): 12277–12290. DOI: https://dx.doi.org/10.1029/2018JD028954.

Flanner, MG, **Zender, CS**, **Randerson, JT**, **Rasch, PJ**. 2007. Present-day climate forcing and response from black carbon in snow. *Journal of Geophysical Research: Atmospheres* **112**(D11): 202. DOI: https://dx.doi.org/10.1029/2006JD008003.

Gardner, AS, **Sharp, MJ**. 2010. A review of snow and ice albedo and the development of a new physically based broadband albedo parameterization. *Journal of Geophysical Research* **115**: F01009. DOI: https://dx.doi.org/10.1029/2009JF001444.

Gertler, CG, **Puppala, SP**, **Panday, A**, **Stumm, D**, **Shea, J**. 2016. Black carbon and the Himalayan cryosphere: A review. *Atmospheric Environment* **125**: 404–417. DOI: https://dx.doi.org/10.1016/j.atmosenv.2015.08.078.

He, C, **Flanner, MG**, **Chen, F**, **Barlage, M**, **Liou, K-N**, **Kang, S**, **Ming, J**, **Qian, Y**. 2018. Black carbon-induced snow albedo reduction over the Tibetan Plateau: Uncertainties from snow grain shape and aerosol–snow mixing state based on an updated SNICAR model. *Atmospheric Chemistry and Physics* **18**: 11507–11527. DOI: https://dx.doi.org/10.5194/acp-18-11507-2018.

Helfricht, K, **Hartl, L**, **Koch, R**, **Marty, C**, **Olefs, M**. 2018. Obtaining sub-daily new snow density from automated measurements in high mountain regions. *Hydrology and Earth System Sciences* **22**: 2655–2668. DOI: https://dx.doi.org/10.5194/hess-22-2655-2018.

Hulstrom, R, **Bird, R**, **Riordan, C**. 1985. Spectral solar irradiance data sets for selected terrestrial conditions. *Solar Cells* **15**: 365–391.

Jacobi, H-W, **Lim, S**, **Ménégoz, M**, **Ginot, P**, **Laj, P**, **Bonasoni, P**, **Stocchi, P**, **Marinoni, A**, **Arnaud, Y**. 2015. Black carbon in snow in the upper Himalayan Khumbu Valley, Nepal: Observations and modeling of the impact on snow albedo, melting, and radiative forcing. *The Cryosphere* **9**: 1685–1699. DOI: https://dx.doi.org/10.5194/tc-9-1685-2015.

Lazarcik, J, **Dibb, JE**, **Adolph, AC**, **Amante, JM**, **Wake, CP**, **Scheuer, E**, **Mineau, MM**, **Albert, MR**. 2017. Major fraction of black carbon is flushed from the melting New Hampshire snowpack nearly as quickly as soluble impurities. *Journal of Geophysical*

Downloaded from http://online.ucpress.edu/elementa/article-pdf/10/1/00118/716484/elementa.2021.00118.pdf by guest on 14 August 2024

Research: Atmospheres **122**: 537–553. DOI: https://dx.doi.org/10.1002/2016JD025351.

Li, X, **Kang, S**, **Zhang, G**, **Que, B**, **Tripatheea, L**, **Paudyal, R**, **Jing, Z**, **Zhang, Y**, **Yan, F**, **Li, G**, **Cui, X**, **Xu, R**, **Hu, Z**, **Li, C**. 2018. Light-absorbing impurities in a southern Tibetan Plateau glacier: Variations and potential impact on snow albedo and radiative forcing. *Atmospheric Research* **200**: 77–87. DOI: https://dx.doi.org/10.1016/j.atmosres.2017.10.002.

Meinander, O, **Kazadzis, S**, **Arola, A**, **Riihelä, A**, **Räisänen, P**, **Kivi, R**, **Kontu, A**, **Kouznetsov, R**, **Sofiev, M**, **Svensson, J**, **Suokanerva, H**, **Aaltonen, V**, **Manninen, T**, **Roujean, J-L**, **Hautecoeur, O**. 2013. Spectral albedo of seasonal snow during intensive melt period at Sodankylä, beyond the Arctic Circle. *Atmospheric Chemistry and Physics* **13**: 3793–3810. DOI: https://dx.doi.org/10.5194/acp-13-3793-2013.

Mimeau, L, **Esteves, M**, **Zin, I**, **Jacobi, H-W**, **Brun, F**, **Wagnon, P**, **Koirala, D**, **Arnaud, Y**. 2019. Quantification of different flow components in a high-altitude glacierized catchment (Dudh Koshi, Himalaya): Some cryospheric-related issues. *Hydrology and Earth System Sciences* **23**: 3969–3996. DOI: https://dx.doi.org/10.5194/hess-23-3969-2019.

Niwano, M, **Kajino, M**, **Kajikawa, T**, **Aoki, T**, **Kodama, Y**, **Tanikawa, T**, **Matoba, S**. 2021. Quantifying relative contributions of light-absorbing particles from domestic and foreign sources on snow melt at Sapporo, Japan during the 2011–2012 winter. *Geophysical Research Letters* **48**(16): e2021GL093940. DOI: https://dx.doi.org/10.1029/2021GL093940.

Onuma, Y, **Takeuchi, N**, **Tanaka, S**, **Nagatsuka, N**, **Niwano, M**, **Aoki, T**. 2020. Physically based model of the contribution of red snow algal cells to temporal changes in albedo in northwest Greenland. *Cryosphere* **14**: 2087–2101. DOI: https://dx.doi.org/10.5194/tc-14-2087-2020.

Painter, TH, **Molotch, NP**, **Cassidy, M**, **Flanner, M**, **Steffen, K**. 2007. Contact spectroscopy for determination of stratigraphy of optical grain size. *Journal of Glaciology* **53**: 121–127. DOI: https://dx.doi.org/10.3189/172756507781833947.

Pedersen, CA, **Gallet, J-C**, **Ström, J**, **Gerland, S**, **Hudson, SR**, **Forsström, S**, **Isaksson, E**, **Berntsen, TK**. 2015. In situ observations of black carbon in snow and the corresponding spectral surface albedo reduction. *Journal of Geophysical Research: Atmospheres* **120**: 1476–1489. DOI: https://dx.doi.org/10.1002/2014JD022407.

Pedersen, CA, **Winther, J**. 2005. Intercomparison and validation of snow albedo parameterization schemes in climate models. *Climate Dynamics* **25**: 351–362. DOI: https://dx.doi.org/10.1007/s00382-005-0037-0.

Reveillet, M, **Dumont, M**, **Gascoin, S**, **Lafaysse, M**, **Nabat, P**, **Ribes, A**, **Nheili, R**, **Tuzet, F**, **Menegoz, M**, **Morin, S**, **Picard, G**, **Ginoux, P**. 2021. Black carbon and dust alter the response of mountain snow cover under climate change, in review. *Earth-Science Reviews* **210**. DOI: https://dx.doi.org/10.21203/rs.3.rs-800501/v1.

Roeckner, E, Bauml, G, Bonaventura, L, Brokopf, R, Esch, M, Giorgetta, M, Hagemann, S, Kirchner, I, Kornblueh, L, Manzini, E, Rhodin, A, Schlese, U, Schulzweida, U, Tompkins, A. 2003. The atmospheric general circulation model ECHAM5, Part I, Model description. Max Planck Institute for Meteorology. Report 349. ISSN 0937-1060. Available at http://www.mpimet.mpg.de/fileadmin/models/echam/mpireport349.pdf.

Roesch, A, Roeckner, E. 2006. Assessment of snow cover and surface albedo in the ECHAM5 general circulation model. *Journal of Climate* **19**: 3828–3843.

Sarangi, C, **Qian, Y**, **Rittger, K**, **Leung, R**, **Chand, D**, **Bormann, KJ**, **Painter, TH**. 2020. Dust dominates high-altitude snow darkening and melt over high-mountain Asia. *Nature Climate Change* **10**: 1045–1051. DOI: https://dx.doi.org/10.1038/s41558-020-00909-3.

Schmale, J, **Flanner, M**, **Kang, S**, **Sprenger, M**, **Zhang, Q**, **Guo, J**, **Li, Y**, **Schwikowski, M**, **Farinotti, D**. 2017. Modulation of snow reflectance and snowmelt from Central Asian glaciers by anthropogenic black carbon. *Scientific Reports* **7**: 40501. DOI: https://dx.doi.org/10.1038/srep40501.

Skiles, SM, **Painter, TH**. 2017. Daily evolution in dust and black carbon content, snow grain size, and snow albedo during snowmelt, Rocky Mountains, Colorado. *Journal of Glaciology* **63**: 118–132. DOI: https://dx.doi.org/10.1017/jog.2016.125.

Skiles, SM, **Painter, TH**. 2019. Toward understanding direct absorption and grain size feedbacks by dust radiative forcing in snow with coupled snow physical and radiative transfer modeling. *Water Resources Research* **55**: 7362–7378. DOI: https://dx.doi.org/10.1029/2018WR024573.

Skiles, SM, **Painter, TH**, **Deems, J**, **Landry, C**, **Bryant, A**. 2012. Dust radiative forcing in snow of the Upper Colorado River Basin. Part II: Interannual variability in radiative forcing and snowmelt rates. *Water Resources Research* **48**: W07522.

Sterle, KM, **McConnell, JR**, **Dozier, J**, **Edwards, R**, **Flanner, MG**. 2013. Retention and radiative forcing of black carbon in eastern Sierra Nevada snow. *The Cryosphere* **7**: 365–374. DOI: https://dx.doi.org/10.5194/tc-7-365-2013.

Svensson, J, **Ström, J**, **Honkonen, H**, **Asmi, E**, **Dkhar, NB**, **Tayal, S**, **Sharma, VP**, **Hooda, R**, **Leppäranta, M**, **Jacobi, H-W**, **Lihavainen, H**, **Hyvärinen, A**. 2021. Deposition of light-absorbing particles in glacier snow of the Sunderdhunga valley, the southern forefront of Central Himalaya. *Atmospheric Chemistry and Physics* **21**: 2931–2943. DOI: https://dx.doi.org/10.5194/acp-21-2931-2021.

Svensson, J, **Ström, J**, **Kivekäs, N**, **Dkhar, NB**, **Tayal, S**, **Sharma, VP**, **Jutila, A**, **Backman, J**, **Virkkula, A**, **Ruppel, M**, **Hyvärinen, A**, **Kontu, A**, **Hannula, H-R**, **Leppäranta, M**, **Hooda, RK**, **Korhola, A**, **Asmi, E**, **Lihavainen, H**. 2018. Light-absorption of

Downloaded from http://online.ucpress.edu/elementa/article-pdf/10/1/00118/716484/elementa.2021.00118.pdf by guest on 14 August 2024

dust and elemental carbon in snow in the Indian Himalayas and the Finnish Arctic. *Atmospheric Measurement Techniques* **11**: 1403–1416. DOI: https://dx.doi.org/10.5194/amt-11-1403-2018.

Svensson, J, **Virkkula, A**, **Meinander, O**, **Kivekäs, N**, **Hannula, H-R**, **Järvinen, O**, **Peltoniemi, JI**, **Gritsevich, M**, **Heikkilä, A**, **Kontu, A**, **Neitola, K**, **Brus, D**, **Dagsson-Waldhauserova, P**, **Anttila, K**, **Vehkamäki, M**, **Hienola, A**, **de Leeuw, G**, **Lihavainen, H**. 2016. Soot-doped natural snow and its albedo—Results from field experiments. *Boreal Environment Research* **21**: 481–503.

Tuzet, F, **Dumont, M**, **Lafaysse, M**, **Picard, G**, **Arnaud, L**, **Voisin, D**, **Lejeune, Y**, **Charrois, L**, **Nabat, P**, **Morin, S**. 2017. A multilayer physically based snowpack model simulating direct and indirect radiative impacts of light-absorbing impurities in snow. *Cryosphere* **11**: 2633–2653. DOI: https://dx.doi.org/10.5194/tc-11-2633-2017.

Tuzet, F, **Dumont, M**, **Picard, G**, **Lamare, M**, **Voisin, D**, **Nabat, P**, **Lafaysse, M**, **Larue, F**, **Revuelto, J**, **Arnaud, L**. 2020. Quantification of the radiative impact of light-absorbing particles during two contrasted snow seasons at Col du Lautaret (2058 m a.s.l., French Alps). *The Cryosphere* **14**: 4553–4579. DOI: https://dx.doi.org/10.5194/tc-14-4553-2020.

Warren, S, **Wiscombe, W**. 1980. A model for the spectral albedo of snow. II: Snow containing atmospheric aerosols. *Journal of Atmospheric Sciences* **37**(12): 2734–2745.

Winter, J-G. 1993. Short- and long-term variability of snow albedo. *Nord Hydrology* **24**: 199–212.

Xu, B, **Cao, J**, **Joswiak, DR**, **Liu, X**, **Zhao, H**, **He, J**, **Zhang, Y**, **Shiyin, L**, **Yongjian, D**. 2012. Post-depositional enrichment of black soot in snow-pack and accelerated melting of Tibetan glaciers. *Environmental Research Letters* **7**(1): 014022. DOI: https://dx.doi.org/10.1088/1748-9326/7/1/014022.

Zhang, Y, **Kang, S**, **Sprenger, M**, **Cong, Z**, **Gao, T**, **Li, C**, **Tao, S**, **Li, X**, **Zhong, X**, **Xu, M**, **Meng, W**, **Neupane, B**, **Qin, X**, **Sillanpää, M**. 2018. Black carbon and mineral dust in snow cover on the Tibetan Plateau. *Cryosphere* **12**: 413–431. DOI: https://dx.doi.org/10.5194/tc-12-413-2018.

Downloaded from http://online.ucpress.edu/elementa/article-pdf/10/1/00118/716484/elementa.2021.00118.pdf by guest on 14 August 2024

How to cite this article: Ström, J, Svensson, J, Honkanen, H, Asmi, E, Dkhar, NB, Tayal, S, Sharma, VP, Hooda, R, Meinander, O, Leppäranta, M, Jacobi, H-W, Lihavainen, H, Hyvärinen, A. 2022. Snow albedo and its sensitivity to changes in deposited light-absorbing particles estimated from ambient temperature and snow depth observations at a high-altitude site in the Himalaya. *Elementa: Science of the Anthropocene* 10(1). DOI: https://doi.org/10.1525/elementa.2021.000118

Domain Editor-in-Chief: Detlev Helmig, Boulder AIR LLC, Boulder, CO, USA

Associate Editor: Hélène Angot, Extreme Environments Research Laboratory, Ecole Polytechnique Fédérale de Lausanne (EPFL), Switzerland

Knowledge Domain: Atmospheric Science

Published: June 10, 2022 **Accepted:** May 14, 2022 **Submitted:** December 14, 2021

Copyright: © 2022 The Author(s). This is an open-access article distributed under the terms of the Creative Commons Attribution 4.0 International License (CC-BY 4.0), which permits unrestricted use, distribution, and reproduction in any medium, provided the original author and source are credited. See http://creativecommons.org/licenses/by/4.0/.

ELEMENTA Science of the Anthropocene

Elem Sci Anth is a peer-reviewed open access journal published by University of California Press.

OPEN ACCESS